

Galaxy disc central surface brightness distribution in the optical and near-infrared bands

L. Zhou^{1,2,3*}, W. Du^{2†}, H. Wu^{2‡}, Y. C. Liang², M. He^{2,3}, P. S. Zhao^{2,3},
L. C. Deng², W. B. Shi^{1,2§}, Y. H. Wang^{2,3}

¹Shandong Provincial Key Laboratory of Optical Astronomy and Solar-Terrestrial Environment,
School of Space Science and Physics, Shandong University at Weihai, Weihai 264209, China

²Key Laboratory of Optical Astronomy, National Astronomical Observatories, Chinese Academy of Sciences,
20A Datun Road, Chaoyang District, Beijing 100012, China

³School of Astronomy and Space Science, University of the Chinese Academy of Sciences, Beijing 101408, China

Accepted XXX. Received YYY; in original form ZZZ

ABSTRACT

To study the disc central surface brightness (μ_0) distribution in optical and near-infrared bands, we select 708 disc-dominated galaxies within a fixed distance of 57 Mpc from SDSS DR7 and UKIDSS DR10. Then we fit μ_0 distribution by using single and double Gaussian profiles with an optimal bin size for the final sample of 538 galaxies in optical *griz* bands and near-infrared *YJHK* bands.

Among the 8 bands, we find that μ_0 distribution in optical bands can not be much better fitted with double Gaussian profiles. However, for all the near-infrared bands, the evidence of being better fitted by using double Gaussian profiles is positive. Especially for *K* band, the evidence of a double Gaussian profile being better than a single Gaussian profile for μ_0 distribution is very strong, the reliability of which can be approved by 1000 times test for our sample. No dust extinction correction is applied. The difference of μ_0 distribution between optical and near-infrared bands could be caused by the effect of dust extinction in optical bands. Due to the sample selection criteria, our sample is not absolutely complete. However, the sample incompleteness does not change the double Gaussian distribution of μ_0 in *K* band. Furthermore, we discuss some possible reasons for the fitting results of μ_0 distribution in *K* band. Conclusively, the double Gaussian distribution of μ_0 in *K* band for our sample may depend on bulge-to-disk ratio, color and disk scalelength, rather than the inclination of sample galaxies, bin size and statistical fluctuations.

Key words: Galaxies: fundamental parameters – Galaxies: photometry – Galaxies: structure – Galaxies: evolution

1 INTRODUCTION

The distributions of different galaxy parameters in different environments could provide important constraints for setting up theoretical models of galaxy formation and evolution (e.g. Thompson 2003). There are some works which found bimodal distributions of galaxy parameters, such as color (e.g. Baldry et al. 2004, Martínez et al. 2006, Brammer et al. 2009, Whitaker et al. 2011), star formation rate (Wetzell et al. 2012), and disc central surface brightness (μ_0 ; e.g. Tully

& Verheijen 1997, McDonald et al. 2009a, McDonald et al. 2009b, Sorce et al. 2013 etc.). de Vaucouleurs 1948, de Vaucouleurs 1959, Sersic 1968, and Freeman 1970 studied the light profiles of galaxies.

The first work which provided convincing evidence for the bimodal distribution of μ_0 is Tully & Verheijen 1997, which selected 79 sample galaxies from Ursa Major cluster and revealed that there is an apparent lack of intermediate surface brightness galaxies (ISB) in *BRI* and *K'* bands. The separate μ_0 distribution of high (HSB) and low surface brightness (LSB) suggested that there are discrete but stable radial configurations. The authors also pointed that the bimodal distribution of μ_0 could be resulted from the errors induced during fitting galaxy disc process, because the shallow *K'* band could lead to the disc premature truncations

* E-mail: lizhou@bao.ac.cn

† E-mail: wdu@bao.ac.cn

‡ E-mail: hwu@bao.ac.cn

§ E-mail: swb@sdu.edu.cn

and result in the mixture of bulge components. As raised by [Bell & de Blok 2000](#), there is a probability for incorrect inclination corrections and small-number statistics to result in the bimodality of μ_0 distribution.

To overcome the error induced by small-number statistics, [McDonald et al. 2009b](#) selected a larger number of sample galaxies (286 galaxies) from Virgo cluster and also found a μ_0 bimodal distribution. However, they claimed that only Virgo cluster has been studied, so they inferred that the bimodality of μ_0 could not be intrinsic and the μ_0 distribution could be different in different environment. [Sorice et al. 2013](#) selected 438 galaxies from Spitzer Survey of Stellar Structure in Galaxies (*S⁴G*) by limiting with distance and morphology type. They demonstrated that there is a bimodality in μ_0 distribution, which implies that there is a gap between LSB galaxies and HSB galaxies. They investigated some possible reasons that would lead to the bimodality, such as small-number statistics, environment influences, low signal-to-noise (S/N) and galaxy inclination correction, and found the bimodality of μ_0 cannot be due to any of these biases or statistical fluctuations. In [Sorice et al. 2016](#), they showed that there is no bimodality of the central surface brightness for galaxies in sheets, while there is bimodality in voids and filaments. [Sorice et al. 2013](#) extended the study outside of clusters and found that there is still bimodality for the overall sample composed of galaxies inside and outside of clusters. Therefore, bimodality found in clusters is not only a cluster feature. [Sorice et al. 2016](#) pushed the limit further by splitting sample using the cosmic web and found that indeed bimodality is not only a cluster but also a filament and void feature, while it is not a sheet feature. They suggested that there may be two stable states of galaxy being: LSB galaxies are dominated by dark matter component and HSB galaxies are dominated by baryonic matter in the center. The reason for the low number of ISB galaxies could be that the co-dominated situation of baryonic and dark matter in the center is not stable.

According to previous studies, we would like to study μ_0 distribution of a sample of galaxies using data from SDSS and UKIDSS. This paper is organized as follows: In section 2, we describe the sample selections. The photometry and geometric fitting are shown in Section 3. The distributions of surface brightness in different bands are shown in section 4. Finally, we discuss our results in section 5 and give conclusions in section 6. Throughout this paper, we adopt a cosmological model with $H_0=70\text{km s}^{-1}\text{Mpc}^{-1}$, $\Omega_M=0.3$, $\Omega_\Lambda=0.7$. We use AB magnitudes for Sloan Digital Sky Survey (SDSS) and Vega magnitudes for United Kingdom Infra-Red Telescope (UKIRT) Infrared Deep Sky Survey (UKIDSS).

2 DATA

2.1 SDSS DR7

Using a dedicated wide-field 2.5-meter telescope at Apache Point Observatory in New Mexico, SDSS([Gunn et al. 1998](#), [York et al. 2000](#), [Lupton et al. 2001](#), [Strauss et al. 2002](#), [Stoughton et al. 2002](#)) is intended to map one quarter of the whole sky($\sim 10,000\text{deg}^2$) with CCD imaging in five bands (u, g, r, i, z) and spectroscopy ranging from 3800 to 9200 Å for millions of galaxies, quasars and stars. All the

sample galaxies used in this work are drawn from the main galaxy sample of SDSS Data Release 7 (DR7) ([Abazajian et al. 2009](#)). The main galaxy sample is comprised of galaxies with r – band Petrosian magnitude brighter than 17.77 mag ([Strauss et al. 2002](#)). In the SDSS DR7 image catalogue, there are 11,663 deg^2 of imaging data. For u, g, r, i and z bands, the 95% completeness magnitude limits are 22.0, 22.2, 22.2, 21.3 and 20.5 mag, respectively ([Abazajian et al. 2004](#)).

2.2 UKIDSS LAS DR10

The UKIRT UKIDSS has been carried out using the Wide Field Camera (WFCAM; [Casali et al. 2007](#)), which has a field of view of 0.21 deg^2 and a pixel size of 0.4 *arcsecond* on the 3.8-meter UKIRT. It can be considered as the near-infrared counterpart of the SDSS ([York et al. 2000](#)). There are several surveys in UKIDSS, including the Large Area Survey (LAS), the Galactic Clusters Survey(GCS), the Galactic Plane Survey (GPS), Deep Extragalactic Survey (DXS) and Ultra Deep Survey (UDS), which cover various combinations of the filter set *ZYJHK* with wavelength ranging from 0.83 μm to 2.37 μm and *H₂* ([Lawrence et al. 2007](#)). The area of LAS is about 4000 deg^2 in the Northern Sky. For the four bands (*YJHK*) of LAS, the depths are 20.3, 19.5, 18.6 and 18.2 mag, respectively. The effective volume and the depth of the total UKIDSS is much larger and deeper than the Two-Micron All-Sky Survey (2MASS; [Skrutskie et al. 2006](#)). The primary aim of UKIDSS is to provide a long-term astronomical legacy data base.

2.3 Sample Selection

2.3.1 Sample Selection Method

To obtain reliable and accurate μ_0 of spiral galaxies, we select our sample by limiting distance, fracDev_r and M_r from SDSS DR7 main galaxy sample catalogue and UKIDSS LAS DR10. Our sample selection criteria are as follows:

(1) To obtain more accurate distance, 869,059 galaxies which have non-zero spectroscopic redshifts are selected from SDSS DR7 main galaxy sample.

(2) Then we further select 5,946 galaxies, which have the corrected distance within 57 Mpc to form a volume-limited sample. The method of correcting distance will be described in detail in section 2.3.2.

(3) To ensure that our sample galaxies are disk-dominated galaxies, whose surface brightness profiles could be well described by an exponential profile (e.g. [Bernardi et al. 2005](#), [Chang et al. 2006](#), [Shao et al. 2007](#)), we select 4,725 galaxies which have the bulge-to-total ratios in r band less than 50% ($\text{fracDev}_r \leq 0.5$).

(4) To exclude dwarf galaxies, we select 2,363 galaxies which have r -band magnitudes brighter than 17.77 mag and absolute magnitudes in r -band brighter than -16.0 mag from the previous 4,725 galaxies.

(5) By cross-matching with the UKIDSS LAS DR10 data, those 708 galaxies which have images in all *Y, J, H* and *K* bands are finally selected from the previous 2363 galaxies as our entire sample.

2.3.2 Distance correction and M_r calculation

For galaxies with $z > 0.02$, the distance could be calculated using Doppler redshift formula and Hubble's law directly :

$$V_r = z \times c, \quad (1)$$

and

$$V_r = H_0 \times D, \quad (2)$$

where V_r is radial velocity, D is the distance to the Earth in units of km, z is redshift of the galaxy.

For galaxies with $z \leq 0.02$, we should correct the effect of Virgo cluster on the observed velocity (Mould et al. 2000, Karachentsev & Makarov 1996). We use Eq. (3) in Karachentsev & Makarov 1996 to correct the observed heliocentric velocity to the Earth of our objects to that relative to the centroid of the Local Group, which is:

$$V_{LG} = V_h + V_a(\cos b \cos b_a \cos(l - l_a) + \sin b \sin b_a), \quad (3)$$

where V_{LG} is the velocity corrected to the centroid of the Local Group, V_h is the observed heliocentric velocity estimated using $z \times c$, l and b are the galactic longitude and galactic latitude of the object. For the solar apex with respect to the Local Group galaxies, the parameters we use here ($V_a = 316 \text{ km/s}$, $l_a = 93^\circ$, $b_a = -4^\circ$) are provided by Mould et al. 2000 and Karachentsev & Makarov 1996. Then the Virgo infall is estimated using the infall model described in Schechter 1980. In the model, the estimated radial component (with respect to the Local Group) of peculiar velocity induced by an attractor is,

$$V_{infall} = V_{fid} \cos \theta + V_{fid} \frac{V_o - V_v \cos \theta}{r_{oa}} \left(\frac{r_{oa}}{V_v} \right)^{1-\gamma}, \quad (4)$$

where V_{fid} is the amplitude of the infall pattern to Virgo cluster at the Local Group (here the value is 200 km/s), V_o is the observed velocity of the object in the Local Group frame, V_v is the observed distance of the Virgo cluster expressed as a velocity (here the value is 957 km/s), γ is the slope of the density profile of Virgo cluster (here the value is 2), θ is the projected angle between the object and Virgo cluster, and r_{oa} is the estimated distance of the object from Virgo cluster expressed by velocity,

$$r_{oa} = \sqrt{V_o^2 + V_v^2 - 2V_o V_v \cos \theta}. \quad (5)$$

There are two components in the Eq. (4). The first term is the vector contribution due to the Local Group's peculiar velocity into Virgo cluster, and the second one is the change in the velocity due to the infall of the object into Virgo cluster. Finally, the corrected cosmic velocity with respect to the Local Group is

$$V_{cosmic} = \begin{cases} 957, & \theta \leq 10^\circ, V = 600 \sim 2300 \text{ (6a)} \\ V_{LG} + V_{infall}, & \theta > 10^\circ, V = \text{others.} \end{cases} \quad (6b)$$

Then the luminosity distance of galaxies with $z \leq 0.02$ could be estimated using Eq. (2).

The r -band absolute magnitude M_r is calculated using

$$M_r = m_r + 5 - 5 \times \log_{10} D, \quad (7)$$

where m_r is the apparent magnitude in r band, D is the distance in units of pc estimated by using the corrected velocity and spectroscopic redshift.

2.4 Sample

Finally, by all the criteria, there are 708 galaxies left as our whole sample. The RA and DEC distribution of all the 708 sample galaxies are shown in the left panel of Fig. 1. The relation between redshift and M_r is given in the middle panel of Fig. 1, which shows that redshifts of our sample galaxies range from 0 to 0.014, and the absolute magnitudes in r band satisfy $M_r \leq -16 \text{ mag}$.

Comparing with samples in previous papers such as Tully & Verheijen 1997; McDonald et al. 2009a,b; Sorce et al. 2013, our sample is representative of a slightly different sample of galaxies. Tully & Verheijen 1997 has 62 galaxies in Ursa Major cluster with redshift lower than 0.005, McDonald et al. 2009a,b has 65 and 286 sample galaxies within Ursa Major cluster and Virgo cluster, respectively, and Sorce et al. 2013 has 438 sample galaxies within the distance of 20 Mpc. The redshift and M_B distributions of our sample galaxies and those of McDonald et al. 2009a,b sample are presented in the right panel of Fig. 1. Compared with McDonald et al. 2009a,b, our sample galaxies have a larger range of redshift, which range from 0 to 0.014.

In the Data Analysis section, we will finally obtain 538 galaxies through checking the Galfit fitting models and residual images. The M_r , distance, $fracDev_r$ and color ($g - r$) distributions of 708 entire sample galaxies and 538 analyzed galaxies are presented in Fig. 2. It can be shown from Fig. 2 that the final 538 analyzed galaxies can well represent our entire sample. From the histograms, M_r is limited to -16 mag, distance is limited to 57 Mpc and $fracDev_r$ is limited to 0.5.

3 DATA ANALYSIS

3.1 Photometry

SDSS has already subtracted sky background of images using Photometric Pipeline (PHOTO). This process of sky subtraction is not accurate because it considers the large extended outskirts of bright objects as sky background and lead to sky background overestimation (Lauer et al. 2007, Liu et al. 2008, Hyde & Bernardi 2009, He et al. 2013). In view of this problem, we adopt a more precise method (Zheng et al. 1999, Wu et al. 2002, Du et al. 2015 etc.) to subtract sky background of images in optical and near-infrared bands of our sample galaxies.

For preparation, we derive the corrected frames in g, r, i, z bands from SDSS DR7 and images in Y, J, H, K bands from UKIDSS DR10 LAS for all the 708 sample galaxies. We filter the initial images with a Gaussian function which has a FWHM of 8 pixels, so that we can extend the area of every single object in the initial images to some extent. According to Du et al. 2015, the FWHM value of 8 pixels is much better than any other values for generating a good smoothed image. To avoid missing inner regions and wings of bright objects and faint stellar halos of galaxies, we apply smoothed images with $FWHM = 8$ for SExtractor to detect objects.

Then objects in the smoothed images with peak flux more than 1.5σ above the global sky background value are detected and masked using the software SExtractor (Bertin & Arnouts 1996). As Du et al. 2015 pointed, if we replace the

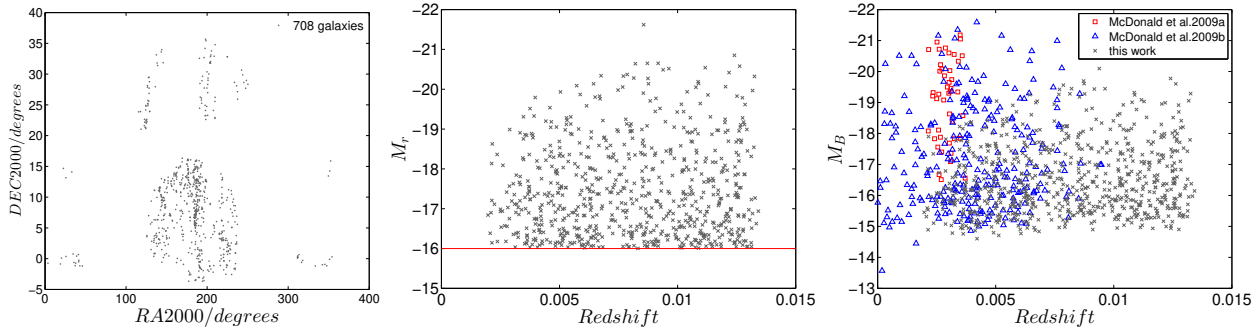


Figure 1. The left panel shows the RA and DEC distributions of our 708 entire sample galaxies. The middle one shows the redshift and absolute magnitude in r band distribution of our entire sample. The red line represents $M_r = -16$ mag. The right panel presents the redshift and absolute magnitude in B band distributions of our entire sample and galaxies from previous studies.

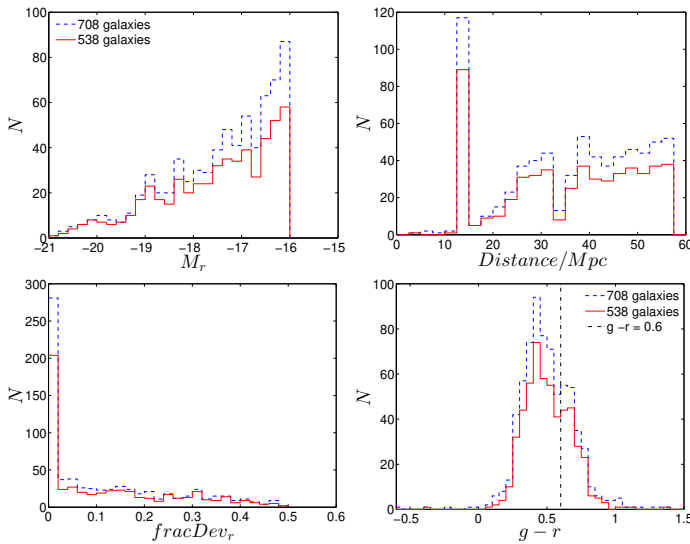


Figure 2. Histograms of different parameters of sample galaxies. In each panel, blue dashed lines represent our entire sample of 708 galaxies, red solid lines represent our final sample of 538 galaxies to be analyzed. Top-left: Absolute magnitude in r band which is limited to -16 mag. Top-right: Corrected distance calculated using spectral redshift, which is limited to 57 Mpc. Bottom-left: $fracDev_r$ value, which is limited to 0.5 to ensure that the bulge contribution to the total luminosity is less than 50%. Bottom-right: color ($g-r$) distribution. $g-r=0.6$ is presented using the black dot-dashed line.

smoothed images with initial images to do object-masking process using SExtractor directly, the wings of bright objects and the faint stellar halos of galaxies may be mistaken as the sky background. The panel *b* in Fig. 3 is the complete masking image for the initial image, which is the panel *a* in Fig. 3. According to the good object-masking images, all objects in the masked area of the initial images are subtracted. In the object-subtracted image, only sky pixels are left. We could derive accurate and reliable sky background from these sky pixels.

At last, the final sky background of the initial image should be modeled using a low order least-squares polynomial fitting process, which is performed row-by-row and column-by-column, to the sky pixels in the object-subtracted image. Also, we average the row-fitted and column-fitted sky

background maps, which is smoothed with the box size of 31×31 pixels to remove any mistakes and make the sky background map more accurate in the modeling process. As Zheng et al. 1999 pointed, the fitting method of straight 2D background fitting may be under-fitted or over-fitted to some areas of images. However, this row-by-row and column-by-column bidirectional fitting method (Zheng et al. 1999, Wu et al. 2002, Lin et al. 2003, Liu et al. 2005, Duan 2006, Liu et al. 2008, Chonis et al. 2011, Mao et al. 2014, Du et al. 2015) is able to forecast the sky background, which is underneath the object-masked areas, in a mutually orthogonal way. Then we should replace the masked object pixels with the fitted values. To avoid introducing spurious fluctuations to the masked areas in the fitted sky background map by interpolations, we restrict the polynomial fits to a low order. The panel *c* of Fig. 3 shows a gradient across the frame. It indicates the smoothed sky background image, which is considered as sky background. The panel *d* of Fig. 3 is the sky-subtracted image of the original image. We have precisely derived the sky background images and subtracted the sky background from the original images of our sample galaxies in multi-bands (g, r, i, z, Y, J, H, K). Fig. 4 shows the count distributions of the image before (top panel) and after (bottom panel) sky subtraction. After sky subtraction, the mean value of ADU is very close to 0.

Here we do surface photometry for the sky-subtracted images of our sample galaxies with the elliptical apertures using the SExtractor software (Bertin & Arnouts 1996). Compared with SDSS Petrosian circular aperture, which is not optimal choice for galaxies with large angular extent, irregular morphology or edge-on shape, the automatic aperture magnitude (AUTO) from SExtractor package could estimate the "total magnitudes" much more precisely. SDSS petrosian aperture could be so large that it includes the light from adjacent objects, or too small to include all the intrinsic light from our target objects.

Automatic aperture magnitudes (AUTO) is inspired by Kron's "first moment" algorithm (Kron 1980). The AUTO aperture R is an elliptical aperture with elongation, ϵ , and position angle, θ , which are defined by the second-order moments of the object's light distribution. Within this aperture, the first moment of an image is defined with

$$R_1 = \frac{\sum RI(R)}{\sum I(R)} \quad (8)$$

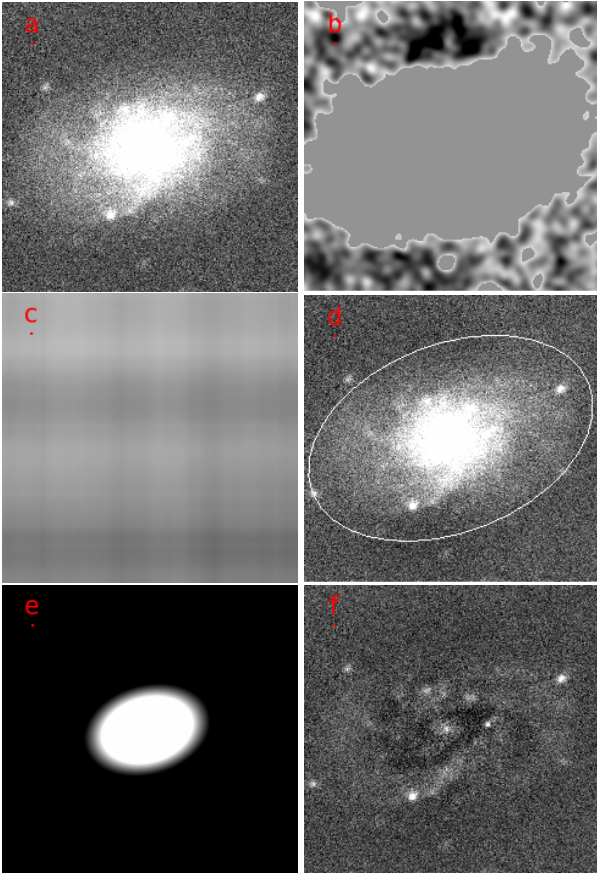


Figure 3. Sky subtraction, photometry and exponential model fitting results for a sample galaxy (objID=587745544271102105) in *g* band. This galaxy locates at the center of this image. The panel *a* is the initial image of this sample. The panel *b* is the complete object masking image. The panel *c* indicates the sky background image from fitting. Kron elliptical aperture (SEx AUTO) for this sample galaxy is presented in panel *d*. Exponential model fitting results for this sample galaxy by Galfit are shown in panel *e* and *f*. The panel *e* presents the exponential profile model and the panel *f* is the residual image, respectively.

According to Kron 1980 and Infante 1987, more than 90% of the flux is expected to lie within an aperture of radius kR_1 for stars and galactic profiles convolved with Gaussian seeing. Here we adopt $k=2.5$ during the automatic elliptical aperture photometry, which is the default setting of SExtractor (Bertin & Arnouts 1996). The panel *d* in Fig. 3 shows the Kron elliptical apertures (SEx AUTO) in the aperture photometry process for the sample galaxy from SDSS DR7 (objID = 587745544271102105) in *g* band. The elliptical aperture is Kron radii. In this way, we could estimate the AUTO magnitude in multi-bands for all our sample galaxies.

3.2 Geometry by Galfit

We use Galfit software (Peng et al. 2002), which is good at galactic geometric fitting, to estimate some useful geometric parameters.

There are several different radial profile functions, e.g., Sersic, exponential, Nuker and other models. Through the sample selection, we remove the bulge-dominated galaxies,

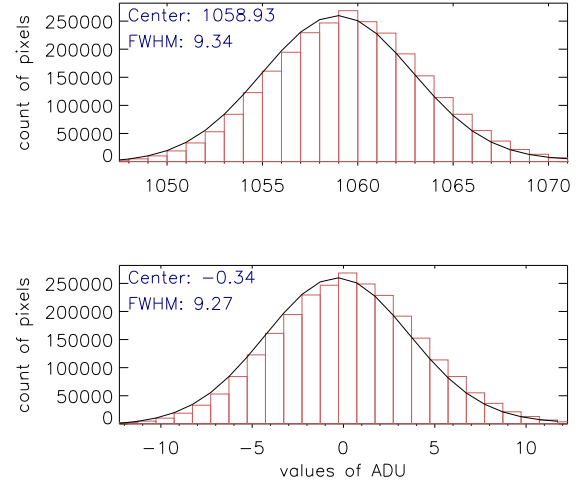


Figure 4. The ADU histogram of the image before (top panel) and after (bottom panel) sky subtraction.

and only disk-dominated galaxies with $\text{fracDev} \leq 0.5$ are left. Therefore, we fit all of our sample galaxies only with exponential profile. The parameters derived from SExtractor photometry process, like galactic magnitude, disk scalelength, axis ratio and position angle, are set as initial input values for the set of Galfit. Then we could derive the best-fit values of parameters, like axis ratio (q), disk scalelength in pixel (α), and inclination angle (i), and also generate three images, including the initial galaxy image, the exponential model (the panel *e* in Fig. 3), and the residual image (the panel *f* in Fig. 3) for each galaxy in our sample.

3.3 Central surface brightness

Normally, μ_0 is used to classify galaxies into low or high surface brightness regime (Freeman 1970, Impey et al. 1996, O’Neil et al. 1997, Zhong et al. 2008, Du et al. 2015). In this subsection, we calculate μ_0 in optical and near-infrared bands for each galaxy in our sample. The surface brightness profiles of disk galaxies could be estimated using an exponential profile:

$$\Sigma(r) = \Sigma_0 \exp(-r/a), \quad a = x \times y, \quad (9)$$

where $\Sigma(r)$ and Σ_0 are the surface brightness in units of $M_\odot \text{pc}^{-2}$ at the radius of r and at the center of the disk, respectively. The parameter of a is the disk scalelength in units of arcsecond. In the description of a , the parameter x is the disk scalelength in units of pixel derived from Galfit, and y is the pixel size in units of arcsec/pixel, which is 0.396 for the SDSS images and 0.4 for UKIDSS LAS DR10 images. Considering the disk of a galaxy is infinite thin, then

$$F_{tot} = 2\pi a^2 \Sigma_0. \quad (10)$$

Combining with

$$F = 10^{-0.4m}, \quad (11)$$

the disc central surface brightness is derived in the form of

$$\mu_0 = m + 2.5 \log(2\pi a^2), \quad (12)$$

where μ_0 is the disc central surface brightness in units of mag arcsec^{-2} , and m means the total apparent magnitude, which is the AUTO aperture magnitude estimated using SExtractor. As O’Neil et al. 1997, Trachternach et al. 2006, Zhong et al. 2008 and Du et al. 2015 pointed out, the central surface brightness should be corrected by inclination and cosmological dimming effects in the form of

$$\mu_0 = m + 2.5 \log_{10}(2\pi a^2 q) - 10 \log_{10}(1 + z). \quad (13)$$

In this equation, q is the axis ratio estimated from the exponential profile fitting by Galfit, and z is the spectral redshift from SDSS DR7. For the multi-bands, we use the same q in r-band to calculate μ_0 . Using this equation, μ_0 in multi-bands (g, r, i, z, Y, J, H, K) are calculated.

We check the Galfit fitting models and residual images of every galaxy in g, r, i, z, Y, J, H and K band. There are 170 galaxies that cannot be fitted well due to the pollution of bright stars or the irregular shape of the galaxy. We remove these 170 badly-fitted galaxies and 538 galaxies are left as our final sample to study the μ_0 distributions. In the final 538 galaxies, there are cluster galaxies and field galaxies.

4 RESULTS

In this section, we examine the μ_0 distributions of our final sample in multi-bands (g, r, i, z, Y, J, H, K) and show them in Fig. 5 with optimal bin size.

We adopt the optimal bin size in each band. According to Freedman & Diaconis 1981, the optimal bin size is $h = 2IQR(X)n^{-1/3}$, where n is the number of observations on X , which is 538 for our sample. $IQR(X)$ is the interquartile range, which is the difference between the upper (top 75%) and lower (bottom 25%) quartiles. A single Gaussian fitting to the distribution is drawn by green lines, while a sum of double Gaussian profiles is described using red solid lines and two separate Gaussian components are described using red dashed-dotted lines.

To estimate the quality of a model and select the best model for a given data, we apply the Akaike information criterion (AIC/AICc) and Bayesian information criterion (BIC) in this work. When the sample size is small, AIC should be corrected into AICc. The likelihood will increase with more parameters added in the process of fitting models, but it could result in over fitting at the same time. Both BIC and AICc attempt to resolve this problem. According to Robert & Adrian. 1995, the model with lower BIC represents better fitting than models with higher BIC. We set $\Delta BIC = BIC_{single} - BIC_{double}$ and $\Delta AICc = AICc_{single} - AICc_{double}$. The evidence that double Gaussian being better than single Gaussian fitting is positive when $2 \leq \Delta BIC$ (or $\Delta AICc$) < 6 , strong when $6 \leq \Delta BIC$ (or $\Delta AICc$) < 10 , and very strong when ΔBIC (or $\Delta AICc$) ≥ 10 .

From all these histograms in Fig. 5 and the values of AICc and BIC in Table 1, it is much better for the μ_0 distribution fitting with a double Gaussian profile than a single Gaussian profile in all the NIR bands (Y, J, H and K band), but it is not in optical bands (g, r, i and z band). The difference of μ_0 distribution between optical and near-infrared bands could be caused by the effect of dust extinction in optical bands. Especially in K band, the evidence of a double

Gaussian profile being better than a single Gaussian profile is very strong, which has $\Delta BIC \geq 10$ and $\Delta AICc \geq 10$. For K band, the μ_0 distribution has double Gaussian peaks with a separation of $\delta\mu_0 \approx 1.8 \text{ mag arcsec}^{-2}$. The double Gaussian peaks are at $\sim 17.4 \text{ mag arcsec}^{-2}$ and $\sim 19.2 \text{ mag arcsec}^{-2}$, respectively. The gap position between two Gaussian peaks in this study locates at $18.3 \text{ mag arcsec}^{-2}$. In Tully & Verheijen 1997, the double Gaussian distribution of μ_0 shows double peaks at 17.3 and $19.7 \text{ mag arcsec}^{-2}$ and the gap position locates at $18.5 \text{ mag arcsec}^{-2}$ in the K' band in the Vega system. In McDonald et al. 2009a and McDonald et al. 2009b, the double peaks locate at about 17.8 and $20 \text{ mag arcsec}^{-2}$ and the gap position locates at $19 \text{ mag arcsec}^{-2}$ in the K' and H band in the Vega system. In AB system, Sorce et al. 2013 has found double peaks at 20.5 and $22.5 \text{ mag arcsec}^{-2}$ and a dearth at $21.5 \text{ mag arcsec}^{-2}$ in the $3.6 \mu\text{m}$ band. The double peak locations and gap positions in this study are similar with those in the previous studies.

5 DISCUSSION

The evidence of a double Gaussian profile being better than a single Gaussian profile for μ_0 distribution is very strong in K band. Therefore, we will discuss possible reasons for the result that the double Gaussian being better than a single Gaussian by taking K band for example. In this section, we analyze the effect of sample incompleteness, axis ratio (b/a), disk scalelength, $fracDev_r$, bin size, color and statistical fluctuations on the μ_0 distribution in K band.

5.1 Effect of sample incompleteness

Our sample is not absolutely complete due to the sample selection criteria. Generally, the criteria in absolute magnitude (brighter than -16 mag in r band) tends to preclude more galaxies with low surface brightness, and our criteria in distance (less than 57 Mpc) and bulge-to-total ratio (less than 0.5) tends to preclude more of the large and bright galaxies, which are generally have high surface brightness. That is to say, it is likely that our selection criteria have only reduced the number of galaxies with low surface brightness and high surface brightness more severely than the number of the galaxies with intermediate surface brightness.

Even by fitting the μ_0 of our sample, which has been flattened at the high and low surface brightness part more largely than the intermediate surface brightness part due to our selection criteria, we could get a double Gaussian fitting in K band, which means the high surface brightness part and low surface brightness part could be separated. So, if the lost galaxies at the high surface brightness and low surface brightness parts could be recovered back into our sample, the peak of the number of galaxies with high or low surface brightness would become more distinct and thus would still show a double Gaussian distribution in central surface brightness in K band.

Therefore, the sample incompleteness does not change our conclusion about double Gaussian distribution of μ_0 in K band.

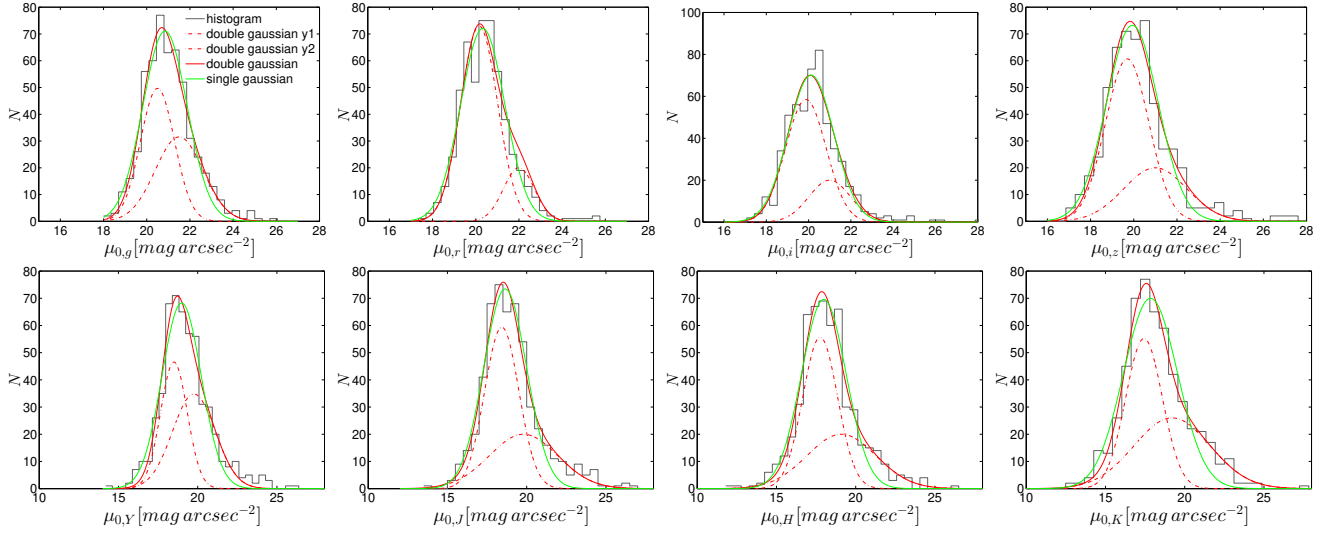


Figure 5. Histograms of μ_0 in multi-bands (g, r, i, z, Y, J, H, K bands) with the optimal bin size. Single Gaussian profile fitting to the distribution is described by green lines, while a sum of double Gaussian profiles is described using red solid lines and two separate Gaussian profiles are described using red dotted lines.

Table 1. The AIC and BIC values of all the sample galaxies with single and double Gaussian fitting with the optimal bin size in multi-bands.

Band	g	r	i	z	Y	J	H	K
AIC_{cs}	69.9	83.7	109.8	85.2	92.6	85.3	100.1	90.8
AIC_{cd}	68.3	96.7	111.5	86.3	87.4	75.5	90.9	61.2
BIC_s	71.8	86.2	113.5	88.0	95.6	88.0	103.2	93.5
BIC_d	69.8	99.7	116.8	90.1	91.5	78.5	94.7	64.2
ΔAIC_c	1.6	-13.0	-1.7	-1.1	5.2	9.8	9.2	29.6
ΔBIC	2.0	-13.5	-3.3	-2.1	4.1	9.5	9.5	29.3
bin size	0.35	0.35	0.36	0.43	0.42	0.50	0.49	0.59

5.2 Inclination

Dust and projection geometry may affect the estimation of μ_0 (Bell & de Blok 2000). As Huizinga 1994 pointed out, when averaging ellipse surfaces at high inclinations, the estimation for the value of μ_0 is systematically smaller than the real value of μ_0 . The assuming of a thin, uniform, slab disc at high inclinations could result in incorrect conclusions due to the effect of three dimensionality of stellar structure on the inclination correction (Sorice et al. 2013). The integration along the line of sight may hide the effects of substructures, like bars and spiral arms (Mosenkov et al. 2010), and there is no precise method to correct the inclination up to now, so it is not easy to estimate accurate μ_0 , especially for edge-on galaxies.

To avoid the effect of incorrect inclination correction to μ_0 , we separate our samples into two parts in terms of inclination, one is galaxies with high inclination ($b/a \leq 0.35$) and the other is galaxies with low inclination ($b/a > 0.35$). The value of 0.35 is adopted by Sorice et al. 2013. According to Figure.2 in Bell & de Blok 2000, the surface brightness distribution of high-inclination galaxies with $b/a \leq 0.4$ has larger error bar and is more inaccurate due to internal extinction. The uncertainties on inclinations are about $4^\circ - 5^\circ$, therefore, choosing 0.35 (73°) instead of 0.4 (69°) will not change the conclusions (Sorice et al. 2013).

The relations between b/a_r and μ_0 in multi-bands are shown in Fig. 6 and distribution of μ_0 for both parts in K band is shown in Fig. 7. In every panel of Fig. 6, R means the correlation coefficient, k means the slope of fitted lines, and std means standard deviation, which are the same as Fig. 8 and Fig. 9. From Fig. 6, the correlation coefficients are lower than 0.2, so there is no apparent correlation between μ_0 and axis ratio.

Fig. 7 is a histogram of the optimal fitting for μ_0 with the optimal bin size in K band for $b/a \leq 0.35$ (blue lines) and $b/a > 0.35$ (red lines), respectively. Given to the incorrect inclination correction for edge-on galaxies, we just ignore the galaxies with $b/a \leq 0.35$ (edge-on galaxies). According to Table 2, the evidence of double Gaussian being better than a single Gaussian for fitting subsample galaxies with $b/a > 0.35$ (low inclinations) is still very strong for the μ_0 distribution in K band.

Therefore, it is not the inclination that lead to the result that double Gaussian being better than a single Gaussian fitting of μ_0 distribution in K band.

5.3 Disk scalelength

The disk scalelength is derived from Galfit fitting procedure result. The correlation coefficients in each panel of Fig. 8

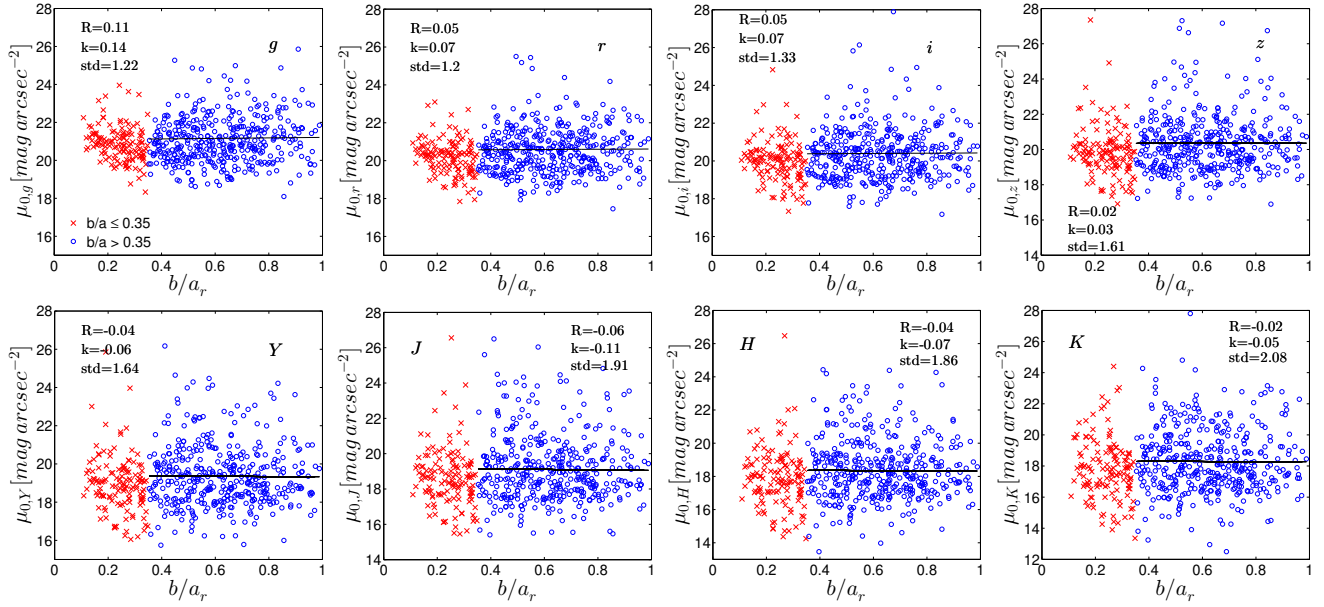


Figure 6. The relations between axial ratio in r-band (b/a_r) and μ_0 in multi-bands (g, r, i, z, Y, J, H, K bands). Red crosses represent highly inclined galaxies with $b/a \leq 0.35$ and blue circles represent less inclined galaxies with $b/a > 0.35$. Black lines represent the fitted lines of less inclined galaxies ($b/a_r > 0.35$). In each panel, R means the correlation coefficient, k means the slope of fitted lines, and std means standard deviation, which are the same as Fig. 8 and Fig. 9.

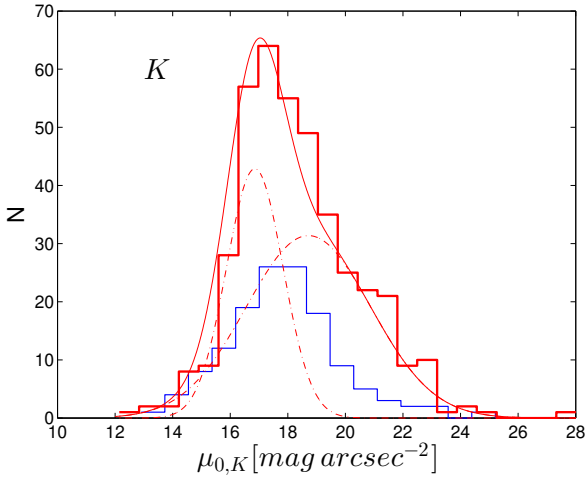


Figure 7. Histograms of the μ_0 distribution with the optimal bin size in K band for galaxies with $b/a \leq 0.35$ (shown with blue thin lines) and $b/a > 0.35$ (shown with red thick lines), respectively. The red dot-dashed lines represent two separate Gaussian components for galaxies with $b/a > 0.35$.

Table 2. The AIC and BIC values of our subsample with $b/a > 0.35$ fitting with single and double Gaussian profiles in K band.

Band	K
AIC_{single}	84.3
AIC_{double}	54.1
BIC_{single}	86.4
BIC_{double}	55.1
ΔAIC	30.2
ΔBIC	31.3

range from 0.2 to 0.5, so there is a weak correlation between μ_0 and disk scalelength in units of kpc. It is clear that LSB galaxies are more extend than HSB galaxies. The μ_0 is larger for galaxies with larger disk scalelength and the galaxies are fainter, and the μ_0 is smaller for galaxies with smaller disk scalelength and the galaxies are brighter.

5.4 Morphology

Decomposition is used to estimate the ratio of bulge light and disk light of galaxies. The definition of $fracDev$ ¹ is as follows:

$$F_{composite} = fracDev F_{dev} + (1 - fracDev) F_{exp}, \quad (14)$$

In this equation, $F_{composite}$, F_{dev} and F_{exp} are the composite, de Vaucouleurs and exponential flux of the object, $fracDev$ is the weight of de Vaucouleurs component in best composite model. The value of $fracDev$ could be obtained from SDSS database. When a galaxy is in the case of $fracDev_r = 0$, it corresponds to pure disk galaxy without a bulge. Here we classify our sample into two subsamples. Subsample 1 is composed of galaxies with $fracDev_r \leq 0.1$ and subsample 2 is composed of galaxies with $0.5 \geq fracDev_r > 0.1$. As McDonald et al. 2009a and McDonald et al. 2009b expected, early-type disc galaxies dominate the HSB peak, while late-type disc galaxies and irregulars are present in both HSB and LSB peaks. The correlation coefficients in each panel of Fig. 9 range from -0.5 to -0.2, so there is a weak negative correlation between μ_0 and $fracDev_r$. It shows that with the increasing of $fracDev_r$, the μ_0 appear to decrease, which means with the increasing of the fraction of bulge light, the galaxies tend to be brighter, which

¹ <http://classic.sdss.org/dr7/algorithms/photometry.html>

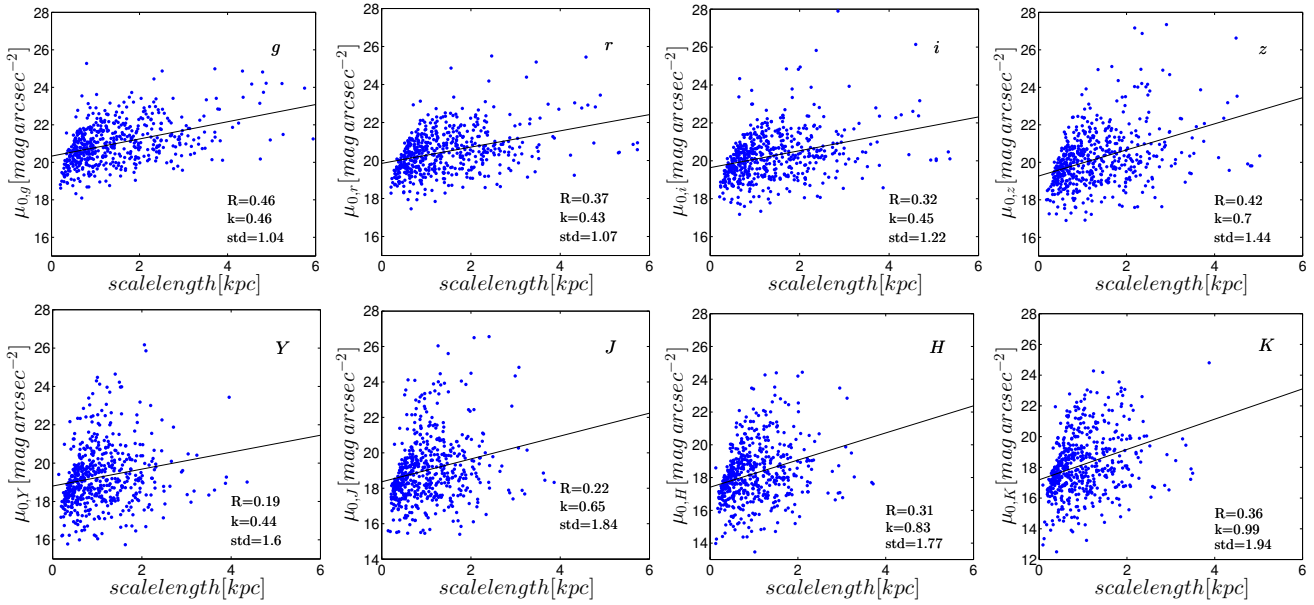


Figure 8. The relations between μ_0 and disk scalelength (in units of kpc) in multi-bands (g, r, i, z, Y, J, H, K bands).

Table 3. The AIC and BIC values of our subsamples with $fracDev_r \leq 0.1$ & $0.5 \geq fracDev_r > 0.1$ fitting with single and double Gaussian profiles in K band.

Value	$fracDev_r \leq 0.1$	$0.5 \geq fracDev_r > 0.1$
AIC_{single}	51.6	47.8
AIC_{double}	51.6	48.2
BIC_{single}	52.3	50.8
BIC_{double}	48.0	51.6
$\Delta AICc$	0.0	-0.4
ΔBIC	4.3	-0.8

is consistent with McDonald et al. 2009a and McDonald et al. 2009b.

The optimal fitting of μ_0 distribution for subsample 1 and subsample 2 in K band are presented in Fig. 10. The location of peaks of μ_0 distribution for subsample 2 (red dashed lines) are smaller than that for subsample 1 (blue dashed lines), which means that disc galaxies with larger fraction of bulge are dominated by galaxies with higher surface brightness and disc galaxies with smaller fraction of bulge are dominated by galaxies with lower surface brightness.

Therefore, there may be some effect for the morphology (disc galaxies with larger or smaller fraction of bulge) on the fact of double Gaussian being better than a single Gaussian fitting for μ_0 distribution in K band.

5.5 Bin size

Considering that the distribution of μ_0 may be influenced by bin size, we change the bin size from 0.2 to 0.9 $mag arcsec^{-2}$ and compare the μ_0 distributions in K band, which is shown in Fig. 11. It reveals that a double Gaussian profile is still much better than a single Gaussian profile for the μ_0 distributions fitting with different bin sizes, which also could be

shown from Table 4 that ΔBIC and $\Delta AICc$ are still larger than 10. The locations of double peak centers for the μ_0 distribution with multi bin sizes are shown in Table 4. The standard deviations for the location of lower surface brightness Gaussian peak and higher surface brightness Gaussian peak are 0.32 and 0.56, respectively.

Therefore, it is not the bin size that leads to the double Gaussian profiles for the distribution of μ_0 in K band.

5.6 Color

To confirm that there are double Gaussian components in K band, we classify our sample into two subsamples, those are bluer galaxies and redder galaxies, and fit them with single and double Gaussian profiles.

The relations between colors and M_K are shown in Fig. 12. The correlation coefficients are -0.76 and -0.40 for relation between $g - K$ and M_K and relation between $g - r$ and M_K , respectively. It is much more correlated between $g - K$ and M_K . In red bands (K band), bluer galaxies (lower value of $g - K$) tend to have fainter magnitude. There is also a tight correlation between color ($g - K$) and μ_0 , which can be shown from the correlation coefficient (-0.83) of the right top panel of Fig. 12. The right bottom panel of Fig. 12 presents the relation between M_g and M_K . The sample could be well separated into two parts by $g - K = -0.55$. The blue crosses in Fig. 12 represent a component of bluer galaxies with $g - K \leq -0.55$ and red circles represent another component of redder galaxies with $g - K > -0.55$.

The left panel of Fig. 13 shows the $fracDev_r$ distribution for bluer galaxies (with $g - K \leq -0.55$) and redder galaxies (with $g - K > -0.55$). The ratios of galaxies with $fracDev \leq 0.1$ for bluer and redder galaxies are 80.5% and 46.7%, respectively. That is to say, bluer galaxies with $g - k \leq -0.55$ contain more galaxies with smaller portion of bulge than redder galaxies.

From the right panel of Fig. 13, for bluer galaxies, the

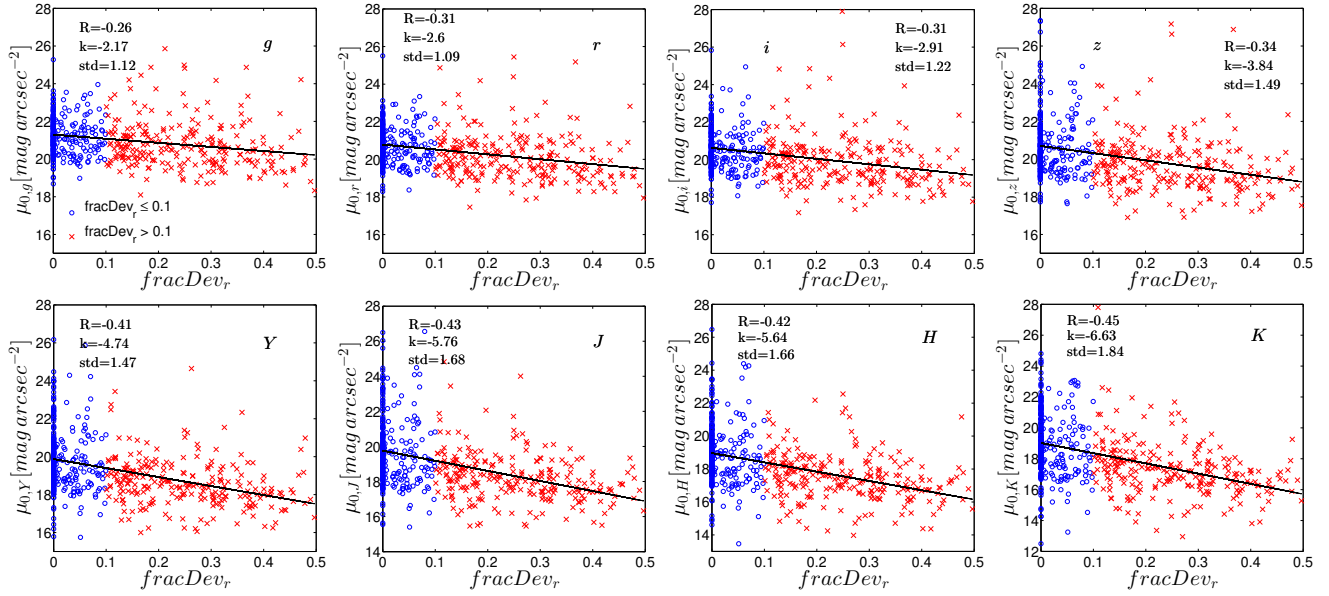


Figure 9. Distributions of μ_0 as a function of $fracDev_r$ for our sample galaxies. Blue circles represent disc galaxies with $fracDev_r \leq 0.1$ and red crosses represent disc galaxies with $0.5 \geq fracDev_r > 0.1$.

Table 4. The AIC and BIC values of all the sample galaxies with single and double Gaussian fitting with multi bin sizes ranging from 0.2 to $0.9 \text{ mag arcsec}^{-2}$ in K band.

bin size	0.2	0.3	0.4	0.5	0.6	0.7	0.8	0.9
AIC_{c_s}	164.3	129.2	128.1	106.9	96.7	90.7	78.2	74.7
AIC_{c_d}	132.1	96.0	106.7	83.1	72.7	73.0	61.3	53.9
BIC_s	171.0	134.4	132.3	110.3	99.4	92.7	79.4	75.4
BIC_d	145.1	105.3	113.2	88.0	75.7	74.0	59.6	51.3
ΔAIC_c	32.2	33.2	21.4	23.8	24.0	17.7	16.9	20.8
ΔBIC	25.9	29.1	19.1	22.3	23.7	18.7	19.8	24.1
μ_1	17.3	17.3	17.3	17.3	17.3	17.3	18.2	17.3
μ_2	19.3	19.4	19.0	19.0	19.1	19.4	20.6	20.0

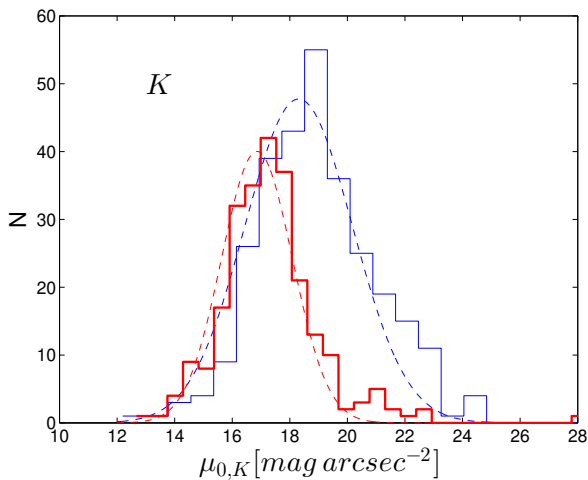


Figure 10. Histograms of the μ_0 distribution with the optimal bin size in K band for galaxies with $fracDev \leq 0.1$ (shown with blue thin lines) and $0.5 \geq fracDev > 0.1$ (shown with red thick lines), respectively.

μ_0 distribution is preferred single Gaussian distribution, but it is not clear for redder galaxies. Similar to the Gaussian fitting results for galaxies with larger or smaller fraction of bulge, there is a difference between the peak centers of μ_0 distribution for bluer and redder galaxies. The peak center of μ_0 distribution for bluer galaxies is larger than that for redder galaxies, that is to say, bluer galaxies tend to have lower surface brightness and redder galaxies tend to have higher surface brightness.

Therefore, there may be some effect for the color (bluer galaxies with $g-k \leq -0.55$ and redder galaxies with $g-K > -0.55$) on the fact of double Gaussian being better than a single Gaussian fitting for μ_0 distribution in K band.

5.7 Statistical fluctuations

The μ_0 distribution of our sample in multi-bands has been presented in the previous Result Section. Especially in K band, the evidence of double Gaussian being better than single Gaussian fitting is very strong. Now we discuss if the result in these bands results from statistical fluctuations. In order to obtain the likelihood of very strong evidence of double Gaussian being better than a single Gaussian fitting,

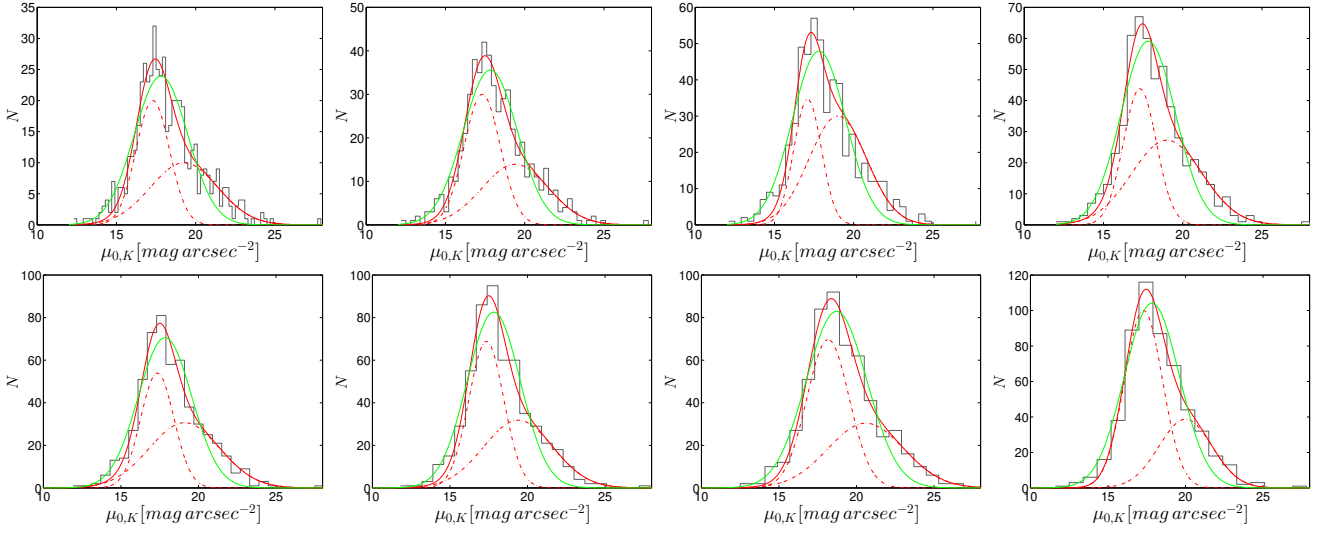


Figure 11. Histograms of the μ_0 distribution in K band with multi bin sizes ranging from 0.2 to 0.9 mag arcsec^{-2} . Single Gaussian fitting to the distribution is described by green lines, while a sum of double Gaussian profiles is described using red solid lines and two separate Gaussian profiles are described using red dotted lines.

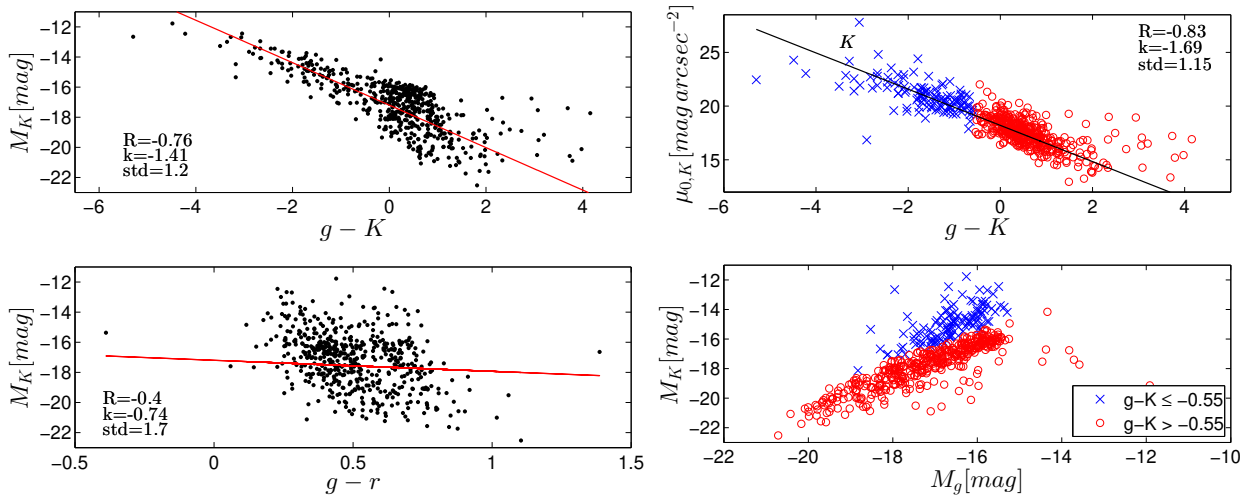


Figure 12. The left top panel represents the relation between the color ($g-K$, which has been translated to AB magnitude) and absolute magnitude in K band (M_K , which has been translated to AB magnitude), and the left bottom panel represents the relation between the color $g-r$ and M_K . The right top panel represents the relation between the color $g-K$ and μ_0 , the right bottom panel represents the relation between absolute magnitude in g band (M_g) and absolute magnitude in K band (M_K).

Table 5. The AIC and BIC values of our subsamples (bluer galaxies with $g-K \leq -0.55$ and redder galaxies with $g-K > -0.55$) fitting with single and double Gaussian profiles in K band.

Value	$g-K \leq -0.55$	$g-K > -0.55$
AIC_{single}	42.2	62.1
AIC_{double}	74.1	65.4
BIC_{single}	42.6	63.6
BIC_{double}	73.2	64.4
$\Delta AICc$	-31.9	-3.3
ΔBIC	-30.6	-0.8

we randomly select the same number of galaxies from our sample, and every single galaxy could be selected any times.

We repeat 1000 times using both double Gaussian fitting and single Gaussian fitting. Here we also apply AICc and BIC value to estimating the goodness of fitting. If AICc and BIC satisfy:

$$AIC_{c_{single}} - AIC_{c_{double}} \geq 10, \& BIC_{single} - BIC_{double} \geq 10, \quad (15)$$

the evidence of double Gaussian being better than a single Gaussian fitting for μ_0 distribution is considered to be very strong. In the equation, $AIC_{c_{single}}$ and $AIC_{c_{double}}$ are AICc values estimated using single and double Gaussian fitting, respectively. BIC_{single} and BIC_{double} are BIC values estimated using single and double Gaussian fitting, respectively.

Table 6 presents the percent of the very strong evidence

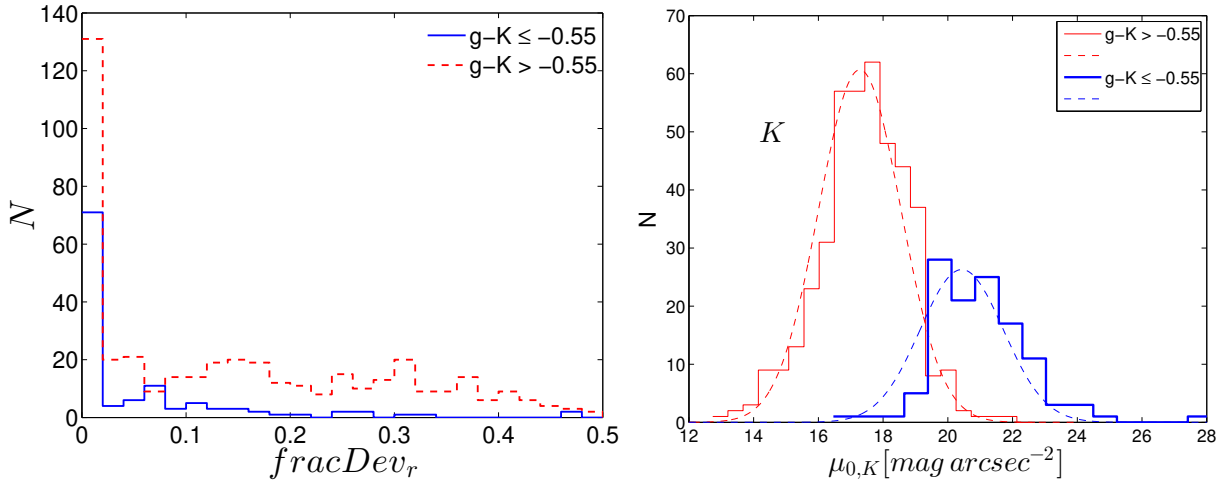


Figure 13. The left panel shows histograms of the fracDev_r distribution for galaxies with $g - K \leq -0.55$ (shown with blue solid lines) and $g - K > -0.55$ (shown with red dashed lines), respectively. The right panel presents histograms of the μ_0 distribution with the optimal bin size in K band for galaxies with $g - K \leq -0.55$ (shown with blue thick lines) and $g - K > -0.55$ (shown with red thin lines), respectively.

Table 6. The likelihood of the very strong evidence of double Gaussian being better than a single Gaussian fitting for μ_0 distribution in multi-bands.

Band	g	r	i	z	Y	J	H	K
Percent	6.2	0	0	3.0	11.3	22.1	17.2	78.3

of double Gaussian being better than a single Gaussian fitting for the μ_0 distribution in the 1000 times test. It has the highest probability, 783 out of 1000 tests, to obtain a very strong evidence of a double Gaussian profile being better than a single Gaussian profile for the μ_0 distribution in K band, which is similar to fitting the μ_0 distribution of our sample. For other bands, the percent is much lower.

The results refute the fact that double Gaussian being better than a single Gaussian fitting could be caused by statistical fluctuations.

5.8 What may cause the double Gaussian components in K band?

McDonald et al. 2009a studied the central surface brightness of 65 spiral galaxies in Ursa Major cluster in K' band using bulge and disk decompositions and found a bimodal distribution. The sample size is small and the Ursa Major cluster populations include more early-type galaxies. McDonald et al. 2009b constructed a more complete sample with deep NIR observation of 286 Virgo cluster galaxies, and obtained the same conclusion as the UMa cluster that the central surface brightness distribution is bimodal in H band. Comparing to Tully & Verheijen 1997, McDonald et al. 2009a, McDonald et al. 2009b, which found double peaks at about $18 \text{ mag arcsec}^{-2}$ and $20 \text{ mag arcsec}^{-2}$ and the gap positions at about $19 \text{ mag arcsec}^{-2}$ for galaxies in Virgo cluster and Ursa Major cluster both in K' and H band, the evidence of double Gaussian distribution of μ_0 for our sample is also strong in H and K band, which have double peaks at about 17.8 and $19.2 \text{ mag arcsec}^{-2}$ and gap positions at

about $18.3 \text{ mag arcsec}^{-2}$. It is similar between the double peak locations and gap positions in this study and those in the previous studies. The evidence of double Gaussian being better than single Gaussian fitting is not positive in optical bands, which is consistent with McDonald et al. 2009b. There are double Gaussian components of μ_0 for our galaxies in near-infrared bands (Y , J , H and K band), and the evidence of a double Gaussian profile being better than a single Gaussian profile is very strong in K band, especially.

We discuss and find that the sample incompleteness does not change the μ_0 double Gaussian distribution in K band (More details in Section 5.1.).

To confirm the offset arising from morphological dependencies, we classify our sample into disc galaxies with smaller fraction of bulge ($\text{fracDev}_r \leq 0.1$) and galaxies with larger fraction of bulge ($0.5 \geq \text{fracDev}_r > 0.1$). It confirms that the morphology of galaxies may affect the μ_0 distribution, that is to say, the fact of double Gaussian components may dependent on the morphology of sample galaxies to some extent. According to Fig. 9, disc galaxies with larger fraction of bulge tend to have higher central surface brightness, and disc galaxies with smaller fraction of bulge tend to have lower central surface brightness. Therefore, there is a possibility that disc galaxies with larger and smaller fraction of bulge result in higher and lower central surface brightness peaks, respectively.

According to Fig. 8, there is a weak correlation between disk scalelength and μ_0 . Galaxies with larger disk scalelength tend to be lower surface brightness galaxies, and galaxies with smaller disk scalelength tend to be higher surface brightness galaxies. That's to say, galaxies with larger and smaller disk scalelength may result in lower and higher central surface brightness peaks, respectively.

To confirm that the color of galaxies may affect the μ_0 distribution in K band, we classify our sample into two subsamples, those are bluer galaxies with $g - K \leq -0.55$ and redder galaxies with $g - K > -0.55$, and fit them with single and double Gaussian profiles. From Fig. 12 to Fig. 13, bluer galaxies with $g - K \leq -0.55$ contain more galaxies

with smaller portion of bulge than redder galaxies. Bluer galaxies tend to have lower surface brightness and redder galaxies tend to have higher surface brightness.

To exclude the bias of statistical fluctuations arising by small-number statistics, [Sorce et al. 2013](#) studied the central surface brightness in $3.6 \mu\text{m}$ of 438 galaxies from S^4G . Also, a bimodal distribution is presented. It confirms that the bimodality is independent of statistics. We do 1000 times test and also confirm that the fact of double Gaussian distribution for μ_0 distribution in K band is not caused by statistical fluctuations.

Conclusively, the double Gaussian distribution of μ_0 in K band for our sample may depend on bulge-to-disk ratio, color and disk scalelength, rather than the inclination of sample galaxies, bin size and statistical fluctuations. Higher disc central surface brightness galaxies tend to have larger fraction of bulge and redder color. Lower disc central surface brightness galaxies tend to have smaller fraction of bulge and bluer color. The double Gaussian peak center locations of μ_0 distribution for the final sample are different from those for subsamples with different $fracDev_r$ (galaxies with large fraction of bulge and small fraction of bulge) and subsamples with different color (bluer galaxies with $g - K \leq -0.55$ and redder galaxies with $g - K > -0.55$). Therefore, the double Gaussian distribution of μ_0 in K band for our sample may result from the factors of bulge-to-disk ratio, color and disk scalelength, together.

As explained in [Tully & Verheijen 1997](#) that the source of the bimodality may be an instability for galaxies when the baryons and dark matter are co-dominant in the centers. Galaxies in the high surface brightness part in our sample should be dominated by baryons in the galaxies centers while galaxies in the low surface brightness part in our sample should be dominated by dark matter in the galaxies centers. The galaxies in our sample with intermediate central surface brightness are expected to be unstable because it is an unstable state that baryons and dark matter are co-dominant in the galaxies centers. We intend to center on the work of exploring more possible reasons for bimodality in our future work.

6 CONCLUSION

We analyze 538 galaxies from SDSS DR7 main galaxy catalogue and UKIDSS DR10 LAS to study the disc central surface brightness distributions. It is representative for our sample galaxies within 57 Mpc and absolute magnitude in r band limited to -16 mag. The final sample galaxies lie in clusters and the field. Then GALFIT is used to do exponential profile fittings. When estimating the μ_0 , no correction for dust extinction is applied in this study. The results are concluded as follows:

(1) Among the eight bands in optical and near-infrared, the evidence of double Gaussian being better than a single Gaussian fitting for μ_0 distributions is positive in all near-infrared bands, especially it is very strong in K band, but it is not positive in optical bands. It reveals higher probability of the very strong evidence of double Gaussian being better than a single Gaussian fitting for μ_0 distributions in K band when we repeat 1000 times test, which refutes the hypothesis

that the double Gaussian distribution could be caused by the statistical fluctuations.

(2) Although the final sample is not absolutely complete, the sample incompleteness does not change the double Gaussian distribution of μ_0 in K band for our sample. By analyzing a series of subsamples selected from the final sample, the fact that double Gaussian being much better than a single Gaussian fitting of μ_0 distributions for our sample in K band may be not caused by inclination, bin size and statistical fluctuations.

(3) There is a probability that the fact of double Gaussian being much better than a single Gaussian fitting for μ_0 distributions in K band is caused by the morphology, color and disk scalelength of galaxies. Galaxies with larger fraction of bulge, redder color and smaller disk scalelength may result in higher central surface brightness peak. Galaxies with smaller fraction of bulge, bluer color and larger disk scalelength may result in lower central surface brightness peak. Therefore, the fact of double Gaussian components for μ_0 distribution may be mainly caused by a combination effect of the morphology, color and disk scalelength of sample galaxies.

ACKNOWLEDGMENTS

We appreciate the referee who provided very constructive and helpful comments and suggestions, which helped to improve very well our work. We also thank Fengshan Liu, Chao Liu, Yanbin Yang and Bo Zhang very much for the helpful discussions and comments. This project is supported by the National Natural Science Foundation of China (Grant Nos.11733006, U1531245, 11225316, U1631105). This project is supported by the National Key R&D Program of China (Grant No.2017YFA0402704).

REFERENCES

- Abazajian, K., Adelman-McCarthy, J. K., Agüeros, M. A., et al. 2004, *AJ*, 128, 502
- Abazajian, K. N., Adelman-McCarthy, J. K., Agüeros, M. A., et al. 2009, *ApJS*, 182, 543-558
- Baldry, I. K., Glazebrook, K., Brinkmann, J., et al. 2004, *ApJ*, 600, 681
- Bell, E. F., & de Blok, W. J. G. 2000, *MNRAS*, 311, 668
- Bertin, E., & Arnouts, S. 1996, *A&AS*, 117, 393
- Bernardi, M., Sheth, R. K., Nichol, R. C., Schneider, D. P., & Brinkmann, J. 2005, *AJ*, 129, 61
- Brammer, G. B., Whitaker, K. E., van Dokkum, P. G., et al. 2009, *ApJ*, 706, L173
- Casali, M., Adamson, A., Alves de Oliveira, C., et al. 2007, *A&A*, 467, 777
- Chang, R., Shen, S., Hou, J., Shu, C., & Shao, Z. 2006, *MNRAS*, 372, 199
- Chonis, T. S., Martínez-Delgado, D., Gabany, R. J., et al. 2011, *AJ*, 142, 166
- de Vaucouleurs, G. 1948, *Annales d'Astrophysique*, 11, 247
- de Vaucouleurs, G. 1959, *Handbuch der Physik*, 53, 311
- Du, W., Wu, H., Lam, M. I., et al. 2015, *AJ*, 149, 199
- Duan, Z. 2006, *AJ*, 132, 1581
- Freeman, K. C. 1970, *ApJ*, 160, 811
- Freedman, D., Diaconis, P. 1981, *Zeitschrift für Wahrscheinlichkeitstheorie und Verwandte Gebiete*, doi:<https://doi.org/10.1007/BF01025868>, 57, 453

Gunn, J. E., Carr, M., Rockosi, C., et al. 1998, *AJ*, 116, 3040
 He, Y. Q., Xia, X. Y., Hao, C. N., et al. 2013, *ApJ*, 773, 37
 Huizinga, J. E. 1994, Groningen: Rijksuniversiteit, |c1994
 Hyde, J. B., & Bernardi, M. 2009, *MNRAS*, 394, 1978
 Impey, C. D., Sprayberry, D., Irwin, M. J., & Bothun, G. D. 1996, *ApJS*, 105, 209
 Infante, L. 1987, *A&A*, 183, 177
 Karachentsev, I. D., & Makarov, D. A. 1996, *AJ*, 111, 794
 Kron, R. G. 1980, *ApJS*, 43, 305
 Lauer, T. R., Faber, S. M., Richstone, D., et al. 2007, *ApJ*, 662, 808
 Lawrence, A., Warren, S. J., Almaini, O., et al. 2007, *MNRAS*, 379, 1599
 Lin, W., Zhou, X., Burstein, D., et al. 2003, *AJ*, 126, 1286
 Liu, Y., Zhou, X., Ma, J., et al. 2005, *AJ*, 129, 2628
 Liu, F. S., Xia, X. Y., Mao, S., Wu, H., & Deng, Z. G. 2008, *MNRAS*, 385, 23
 Lupton, R. H., Gunn, J. E., Ivezić, Z., et al. 2001, in *ASP Conf. Proc. 238, Astronomical Data Analysis Software and Systems X*, ed. F. R. Harnden, Jr., F. A. Primini, & H. E. Payne (San Francisco: ASP), 269
 Mao, Y.-W., Kong, X., & Lin, L. 2014, *ApJ*, 789, 76
 Martínez, H. J., O’Mill, A. L., & Lambas, D. G. 2006, *MNRAS*, 372, 253
 McDonald, M., Courteau, S., & Tully, R. B. 2009, *MNRAS*, 393, 628
 McDonald, M., Courteau, S., & Tully, R. B. 2009, *MNRAS*, 394, 2022
 Mosenkov, A. V., Sotnikova, N. Y., & Reshetnikov, V. P. 2010, *MNRAS*, 401, 559
 Mould, J. R., Huchra, J. P., Freedman, W. L., et al. 2000, *ApJ*, 529, 786
 O’Neil, K., Bothun, G. D., & Cornell, M. E. 1997, *AJ*, 113, 1212
 Peng, C. Y., Ho, L. C., Impey, C. D., & Rix, H.-W. 2002, *AJ*, 124, 266
 Kass, Robert E.; Raftery, Adrian E. (1995), "Bayes Factors", *Journal of the American Statistical Association*, 90 (430): 773–795, doi:10.2307/2291091, ISSN 0162-1459.
 Sakamoto, Y., Ishiguro, M., and Kitagawa, G., 1986, *Akaike information criterion statistics*, KTK Scientific Publishers, Tokyo, Japan
 Schechter, P. L. 1980, *AJ*, 85, 801
 Schlegel, D. J., Finkbeiner, D. P., & Davis, M. 1998, *ApJ*, 500, 525
 Sersic, J. L. 1968, Cordoba, Argentina: Observatorio Astronómico, 1968,
 Shao, Z., Xiao, Q., Shen, S., et al. 2007, *ApJ*, 659, 1159
 Skrutskie, M. F., Cutri, R. M., Stiening, R., et al. 2006, *AJ*, 131, 1163
 Sorce, J. G., Courtois, H. M., Sheth, K., & Tully, R. B. 2013, *MNRAS*, 433, 751
 Sorce, J. G., Creasey, P., & Libeskind, N. I. 2016, *MNRAS*, 455, 2644
 Stoughton, C., Lupton, R. H., Bernardi, M., et al. 2002, *AJ*, 123, 485
 Strauss, M. A., Weinberg, D. H., Lupton, R. H., et al. 2002, *AJ*, 124, 1810
 Sugiura, N., Further analysis of the data by Akaike’s information criterion and the finite corrections, *Communications in Statistics, Theory and Methods A7*, 1978, 13–26
 Thompson, R. I. 2003, *Ap&SS*, 284, 353
 Trachternach, C., Bomans, D. J., Haberbettl, L., & Dettmar, R.-J. 2006, *A&A*, 458, 341
 Tully, R. B., & Verheijen, M. A. W. 1997, *ApJ*, 484, 145
 Wetzel, A. R., Tinker, J. L., & Conroy, C. 2012, *MNRAS*, 424, 232
 Whitaker, K. E., Labbé, I., van Dokkum, P. G., et al. 2011, *ApJ*, 735, 86

Wu, H., Burstein, D., Deng, Z., et al. 2002, *AJ*, 123, 1364
 York, D. G., Adelman, J., Anderson, J. E., Jr., et al. 2000, *AJ*, 120, 1579
 Zheng, Z., Shang, Z., Su, H., et al. 1999, *AJ*, 117, 2757
 Zhong, G. H., Liang, Y. C., Liu, F. S., et al. 2008, *MNRAS*, 391, 986

APPENDIX A: AKAIKE INFORMATION CRITERION AND BAYESIAN INFORMATION CRITERION

We use Akaike information criterion (AIC) and Bayesian information criterion (BIC) to select a better model from single and double Gaussian fitting. In the process of model fitting, adding more parameters may increase the likelihood, but it could also bring over fitting problems. To solve this problem, both AIC and BIC introduce a penalty term, which is $\ln(n)$ for BIC and 2 for AIC, for the number of parameters in the model.

The definition of AIC is

$$\text{AIC} = 2k - 2\ln(\hat{L}) \quad (\text{A1})$$

In this equation, k is the number of estimated parameters in the model, which is 3 for a single Gaussian profile and 6 for a double Gaussian profile. \hat{L} is the maximum value of the likelihood function for the model. It is a relative value of the set of models which means differences between AICs rather than the absolute size of AIC value. This is based on the likelihood theory. In the special case of Least Squares (LS) estimation, AIC can be translated into:

$$\text{AIC} = 2k + n\ln(\sigma^2) \quad (\text{A2})$$

In this equation, σ^2 is the estimated variance of a candidate model and n is the number of observed data, which can be estimated using:

$$\sigma^2 = s^2/n, \quad (\text{A3})$$

where s^2 is the residual sum of squares. If the sample size is small compared with the number of parameters, AIC may perform poorly and overfit (Sugiura 1978, Sakamoto 1986). Then AICc is developed with a second-order variant correction of AIC.

$$\text{AICc} = \text{AIC} + (2k^2 + 2k)/(n - k - 1). \quad (\text{A4})$$

Here we use AICc rather than AIC to select models.

The Bayesian information criterion (BIC) is a model selection criteria and based on likelihood function. The definition of BIC is:

$$\text{BIC} = \ln(n)k - 2\ln(\hat{L}) \quad (\text{A5})$$

In Gaussian special case, if the model errors or disturbances are assumed to be independent and identically distributed according to a normal distribution, and the boundary condition that the derivative of the log likelihood with respect to the true variance is zero, this becomes:

$$\text{BIC} = \ln(n)k + n\ln(\sigma^2) \quad (\text{A6})$$

The model with the lowest BIC is preferred when selecting models. With the increasing of the error variance σ^2 and the explained variable k , the value of BIC will increase. Therefore, a model with lower BIC value implies that it may have either fewer explanatory variables, better fit, or both.

Table A1. The strength of the evidence against the model with higher BIC (or AIC) value.

Δ BIC (or Δ AICc)	Evidence against higher BIC (or AICc)
0 to 2	Not worth more than a bare mention
2 to 6	Positive
6 to 10	Strong
≥ 10	Very Strong

The strength of the evidence against the model with higher BIC (or AIC) value can be summarized as Table A1 (Robert & Adrian. 1995).

This paper has been typeset from a $\text{\TeX}/\text{\LaTeX}$ file prepared by the author.